Int J Adv Manuf Technol (2017) 90:2443–2452
DOI 10.1007/s00170-016-9525-0

ORIGINAL ARTICLE

The effect of nanoparticulate loading on the fabrication and characterization of multi-doped Zn-Al2O3-Cr2O3 hybrid coatings on mild steel

N. Malatji[1] · A.P.I. Popoola[1] · O.S.I Fayomi[1,2]

Received: 6 June 2016 / Accepted: 25 September 2016 / Published online: 15 October 2016

Abstract Nanoparticle Al2O3/Cr2O3 was successfully incorporated into Zn rich by electrodeposition technique to produce Zn-Al2O3-Cr2O3 ternary coatings. The morphology and structural characteristics of the fabricated electrodeposits were characterized by scanning electron microscopy (SEM) affixed with energy-dispersive spectroscopy and X-ray diffraction. The electrochemical behavior of the coatings was studied by potentiodynamic polarization. The wear and microhardness properties of the coatings were tested using ball-on-disk sliding wear tester and diamond base microhardness indenter, respectively. The results showed that the incorporation of the nanoparticles into the Zn matrix refines the morphology and modifies the crystallographic orientation of the Zn coatings. The nanocomposite coatings exhibited improved microhardness properties, wear resistance, and thermal stability. Corrosion studies revealed that the incorporation of the mixed-oxide nanoparticles has no significant effect on the corrosion resistance of Zn coatings.

Keywords Electrodeposition · Zn-Cr_2O_3-Al_2O_3 nanocomposite coatings · Corrosion · Thermal stability · Wear

✉ O.S.I Fayomi
ojosundayfayomi3@gmail.com

N. Malatji
doublen.malatji@gmail.com

A.P.I. Popoola
popoolaapi@tut.ac.za

[1] Surface Engineering Research Centre, Department of Chemical, Metallurgical and Materials Engineering, Tshwane University of Technology, Pretoria, South Africa

[2] Department of Mechanical Engineering, Covenant University, Ota, Nigeria

1 Introduction

Advancement in industrial applications of coatings has drastically increased over the last few decades. These increasing demands for coatings that can withstand aggressive environments have led to the search of new coating materials and improvement of existing techniques for fabrication of surface coatings. The required materials need to exhibit excellent anticorrosive, wear resistance, biocompatibility, thermal stability, and printability properties. Incorporation of nanosized particles into metal matrixes poses a promising solution to combat the demand. This is due to the unique and exotic properties possessed by these materials and their ability to perform better than their micron/submicron-sized counterparts [1–3].

Zinc electrodeposition is one of the techniques that have attracted several researchers for the development and fabrication of new novel coatings with functional properties. This owes to the cost-effectiveness, versatility, and simplicity of this technique in the fabrication of surface coatings. Inert nanoparticles such as Al_2O_3, SiO_2, TiO_2, ZrO_2, CeO_2, etc., have been successfully co-deposited with Zn to form Zn nanocomposite coatings [3–6]. Several studies investigated the incorporation of Al_2O_3 and Cr_2O_3 into metal matrixes, and the results showed a positive effect on the surface properties of the coatings. Al_2O_3 and Cr_2O_3 possess excellent corrosion resistance, high hardness, low thermal expansion, and coefficient of friction [6–11].

Inclusion of Al_2O_3 particles into a metal matrix proved to improve the hardness properties of Zn coatings [7]. Blejan et al. investigated the corrosion behavior of Zn-Ni-Al_2O_3 nanocomposite coatings. The presence of alumina nanoparticles in the composite coating showed improved corrosion resistance [9]. The mechanical properties of the composite coatings were also improved when compared to plain Zn coatings [7]. Cr_2O_3 particles alter the surface morphology, increase the hardness, and reduce the corrosion rate of the Ni matrix [11].

Srivastava et al. studied the co-deposition of nickel with Cr_2O_3 nanoparticles in an additive free bath and found that the incorporation of these nanoparticles had no effect on the corrosion resistance of the matrix, but improved the tribological and mechanical properties [8]. The contradictory results obtained for the corrosion resistance of Cr_2O_3 composite coatings indicate that the quality depends on the optimization of the plating parameters.

The inclusion of A_2O_3 and Cr_2O_3 nanoparticles into the metal matrix is available in the published literature. However, investigation of the incorporation of these nanoparticles in a Zn metal matrix is scanty. Therefore, this research seeks to synthesize Zn-Al_2O_3-Cr_2O_3 nanocomposite coatings and study the synergetic effect of Al_2O_3 and Cr_2O_3 nanoparticles in a Zn matrix. The morphology, microstructure, electrochemical, mechanical, and tribological properties of the fabricated coatings were studied.

2 Experimental

2.1 Sample preparation

Zn and Zn-Cr_2O_3-Al_2O_3 nanocomposite coatings were prepared by electrodeposition technique using mild steel plates as cathodes. The mild steel plates were sectioned using a cutting wheel to sections of dimensions of 25 × 40 mm. Emery papers of grit sizes of 180 and 400 grits were used to grind, polish, and remove the unwanted material such as rust on the mild steel substrate. The polished samples were then dipped into ethanol to remove the grease or oil on the mild steel followed by suspension into 1 M HCl to activate the surface prior to plating. The plating solutions were mechanically stirred using a magnetic stirrer for 18 h to keep Cr_2O_3 (100 nm) and Al_2O_3 (50 nm) nanoparticles in suspension (Table 1). During electrodeposition, two Zn plates were used as anodes and the pH was kept constant at 3.8. The deposition time for the experiments was 20 min under ambient conditions while stirring at a speed of 300 rpm. The samples were rinsed in water for 5 s to remove loosely adhered particles and were air-dried after electrodeposition (Table 2).

2.2 Surface characterization

JEOL-JSM-5800V scanning electron microscope was used to study the microstructural characteristics of the as-received powder and electrodeposited samples. The compositional analysis of the samples was done using energy-dispersive spectrometry (EDS) affixed to the microscope. X-ray diffraction (XRD) patterns of the samples were obtained with an XPertPro PANalytical, LR 39487C XRD diffractometer using Cu Kα radiation (40 kV, 40 mA). Stepwise increase for small angle was 0.01° over the range of 1 to 8° and wide angle rate of 1° 2θ min^{-1} over the range of 8 to 90° (2θ). High-resolution 5500LS AFM analytical technique was used to examine the adhesion and topography of fabricated crystalline materials. The topographical images are captioned in 3D dimension through a scanning probe. The amplitude is demonstrated in order of fractions of a nanometer. The methodologies operate at the material interface with a mechanical and piezoelectric probe which facilitates command and enables very precise scanning.

Table 1 Bath composition and operating condition

Composition	Parameters
$ZnCl_2$—150 g/L	Cathode—mild steel
KCl—50 g/L	Anode—Zn
Boric acid—30 g/L	Temperature—25 °C
Glycine—30 g/L	pH—3.8
Thiorea—10 g/L	Current—1.5 A
Cr_2O_3—2.5, 5, 7.5 g/L	
Al_2O_3—2.5, 5, 7.5 g/L	

2.3 Microhardness testing

Diamond indenter microhardness tester was used to investigate the microhardness properties of the samples. The values reported are an average of three indentation measurements made at different locations. The values reported are an average of three indentation measurements made at different locations for a 15-s dwell time with a 100-g load.

2.4 Electrochemical behavior

Electrochemical measurements were performed using μAutolab pontentiostat/galvanostat to investigate the corrosion properties of the samples in a 3.65 % NaCl environment. Saturated calomel electrode was used as a reference and graphite rod as counterelectrode, which were employed for the measurements in a conventional three-electrode electrochemical cell. All the tests were conducted under ambient conditions with specimen of area 1 cm^2 which was exposed to corrosive medium. The potentiodynamic potential scan was fixed from −1.5 V to +1.5 mV with a scan rate of 0.012 V/s. The electrochemical corrosion test was performed at room temperature.

Table 2 Electrodeposited sample codes

Sample code	Description
ZAC1	Zn-2.5 g/L Al_2O_3–7.5 g/L Cr_2O_3
ZAC2	Zn-5 g/L Al_2O_3–5 g/L Cr_2O_3
ZAC3	Zn-7.5 g/L Al_2O_3–2.5 g/L Cr_2O_3

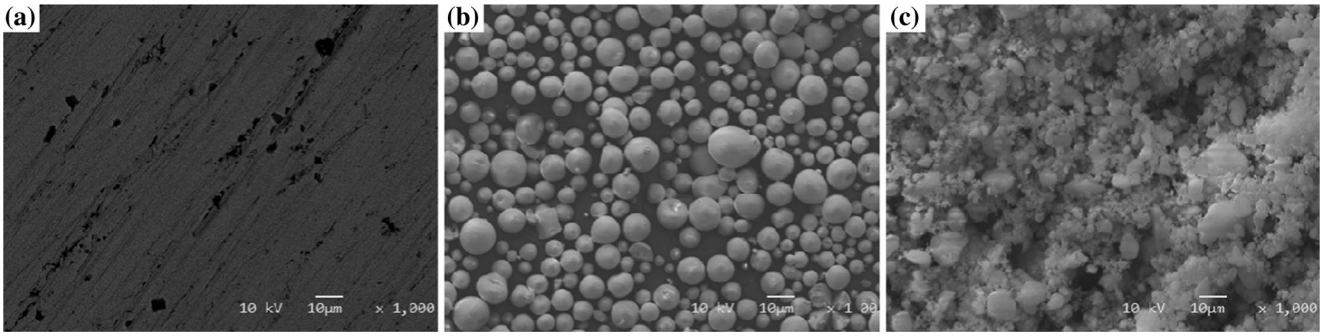

Fig. 1 SEM images for the starting material: **a** as-received powder, **b** Cr_2O_3 nanopowder, and **c** Al_2O_3 nanopowder

2.5 Thermal stability

The coatings were subjected to annealing temperature of 250 °C in a laboratory tube furnace to study their thermal stability. The samples were exposed to heat treatment conditions for a time range of 0.5, 2, and 16 h to study their thermal stability with respect to time for industrial applications where they are required to perform under high temperatures.

2.6 Wear

For wear performance studies, the samples were evaluated using CETR ball-on-disk tribo-tester under dry reciprocating conditions. The coefficient of friction was continually recorded for a duration of 1000 s. All the tests were conducted at a constant normal load of 5 N, sliding velocity of 2 m/s, and sliding distance of 3 mm. The micrographs of the wornout surfaces were observed using scanning electron microscope (×500). Dry abrasion rig machine was used to determine the percentage wear mass loss under dry sliding conditions using silica sand as a wearing medium at a speed of 200 rev/min for 60 s. The initial masses of the samples were weighed before the tests, and the final masses were recorded after the dry sliding. These values were used to determine the percentage wear mass loss.

3 Results and discussion

3.1 Morphological studies

3.1.1 Characterization of the starting materials

The SEM micrographs of the as-received and the metal oxide nanopowders are shown in Fig. 1. The morphology

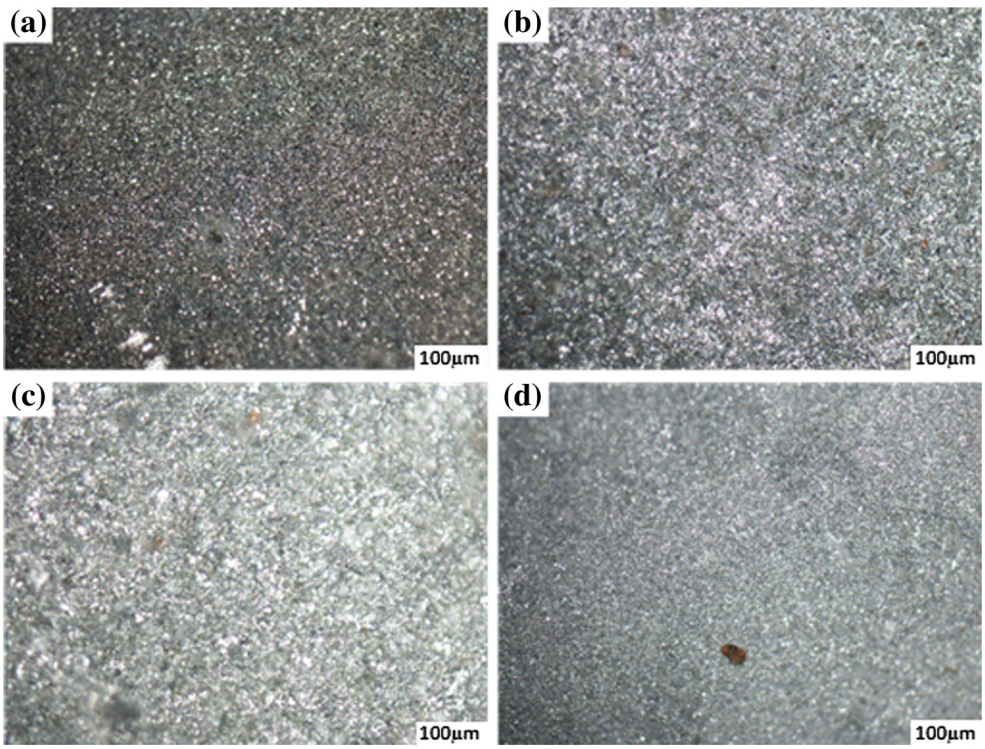

Fig. 2 Optical micrographs of **a** Zn coating, **b** ZAC1 nanocomposite coating, **c** ZAC2 nanocomposite coating, and **d** ZAC3 nanocomposite coating

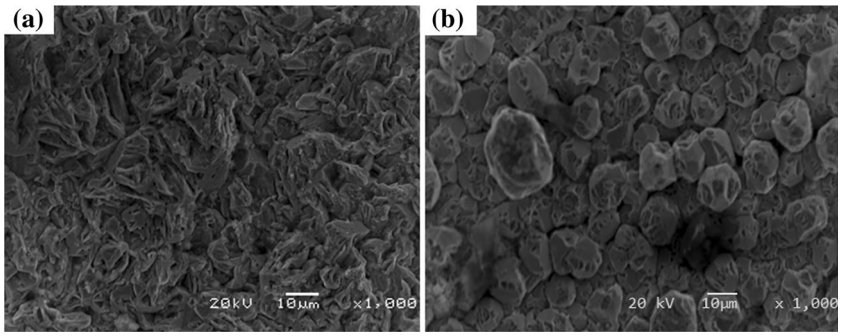

Fig. 3 SEM images of the electrodeposits **a** Zn coating and **b** ZAC1 nanocomposite coating

of mild steel reveals a porous and microholed surface as depicted by Fig. 1a. Al_2O_3 particles (Fig. 1b) show regularly shaped and uniformly dispersed particles. The nature of particles suggests that they can easily be uniformly dispersed in the electroplating bath with no problem of particle agglomeration in moderate stirring rates. However, a clear contrast is seen for Cr_2O_3 which exhibits agglomerated irregularly shaped particles (Fig. 1c).

3.1.2 Optical microscope analysis

The optical microscope micrographs of the Zn and Zn-Al_2O_3-Cr_2O_3 deposited coatings are shown in Fig. 2. ZAC1 (Fig. 2b) and ZAC2 (Fig. 2c) composite coatings contain uniform, compact, and agglomerated crystal grains. The modified microstructure exhibited by these coatings has been induced by the inclusion of the Al_2O_3-Cr_2O_3 mixed composite. The micrographs also reveal that the best altered microstructure due to the incorporation of the nanoparticles have been achieved at particle loading of 5 g/L for both Al_2O_3 and Cr_2O_3 particles. The increase in Al_2O_3 (7.5 g/L) particles and reduction in Cr_2O_3 (2.5 g/L) in the bath gave a similar morphology as that of Zn but with finer grains. This result suggests less incorporation of nanoparticulates into the Zn matrix due to the increment of alumina particles in the bath. The micrographs obtained for the different composites show that the morphological properties of the samples are not affected not only by particle loading but also on the strengthening characteristics of the reinforcement materials.

3.1.3 SEM characterization

Figure 3 shows SEM micrographs of pure Zn coating and ZAC1 nanocomposite coating. SEM analysis was conducted on the sample that exhibited the best electrochemical behavior and Zn coating as a reference. Pure Zn coating reveals flake-like crystals which possess some surface defects such as pores and microholes. On the other hand, the ZAC1 nanocomposite shows uniform and compact granular crystals. This result proves that the incorporation of the nanocomposites into the Zn metal matrix has a significant effect on the morphology of the coatings [17, 18]. The results also confirm the observation made on the optical microscope micrographs. EDS analysis confirmed the presence of Al_2O_3 (1.0 %) and Cr_2O_3 (2.2 %) particles in the coatings as shown in Fig. 4.

3.1.4 Atomic force microscope characterization

3D images for Zn coating and ZAC1 nanocomposite coating obtained from atomic force microscopy are shown in Fig. 5. The Zn matrix possesses irregular and ununiform topography consisting mainly of Zn crystallites. The inuniformity of the Zn matrix surface is caused by generated defects owing to the less controllable crytal growth. The uniform dispersion of particles in the composite coating promotes formation of a fine deposit with excellent topography. Addition of chemical agents has been reported to have a significant effect on the hindered crystal growth of the Zn matrix, and inert oxide particles exhibit similar characteristics [16]. Therefore, inclusion of nanoparticles into a metal matrix produce coatings that possesses limited roughness.

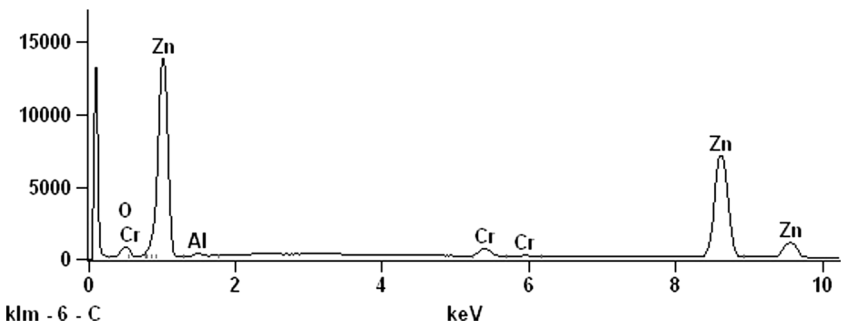

Fig. 4 EDS spectrum of Zn-2.5 g Al_2O_3–7.5 g Cr_2O_3 (ZAC1) nanocomposite coating

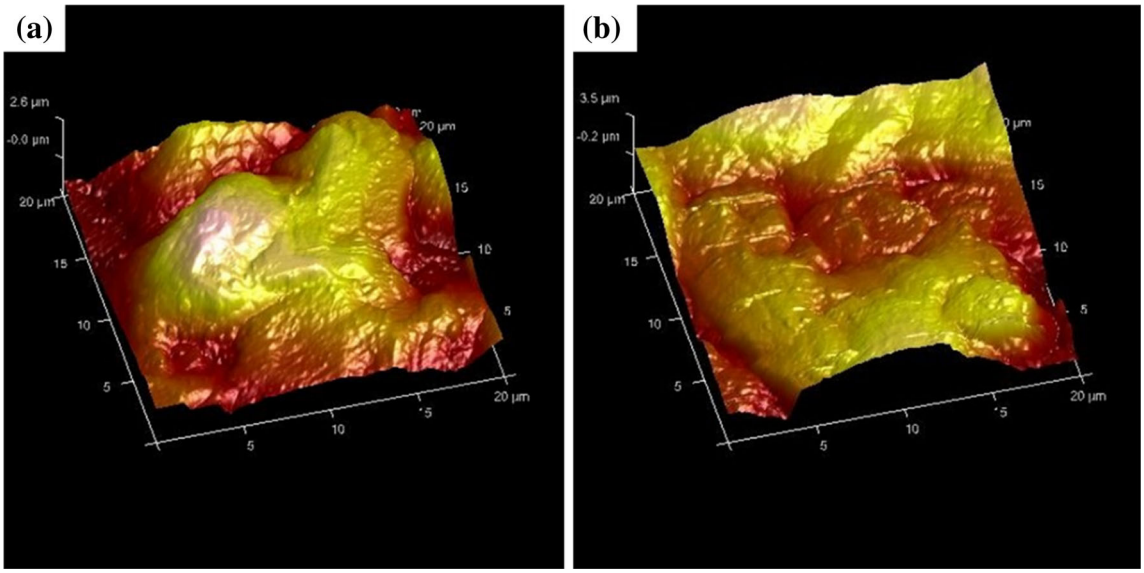

Fig. 5 AFM 3D images of **a** Zn coating and **b** ZAC1 nanocomposite coating

3.2 X-ray diffraction studies

The XRD patterns of electrodeposited Zn and ZAC1 nanocomposite coating are shown in Fig. 6. Majority of the diffraction lines shown by the diffractograms represent the Zn hexagonal structure. The composite coating exhibits a similar structure as the pure Zn coating, but the preferential orientations of the Zn matrix have been modified. The presence of ZnO and Fe peaks were observed on the (110) and (200) planes. The peak intesity of Fe was drastically reduced in the composite coating showing that the incorporation of the nanoparticles provides better deposit to cover the surface of mild steel than Zn. The composite also possesses a peak width that is slightly broader than that of Zn coating. This result can be ascribed to grain size reduction that occurs as a consequence of inert particle incorporation. The adsorption of nanoparticles occurs on the growing crystal and thus inhibits its further growth, causing the formation of a small-sized crystal [4].

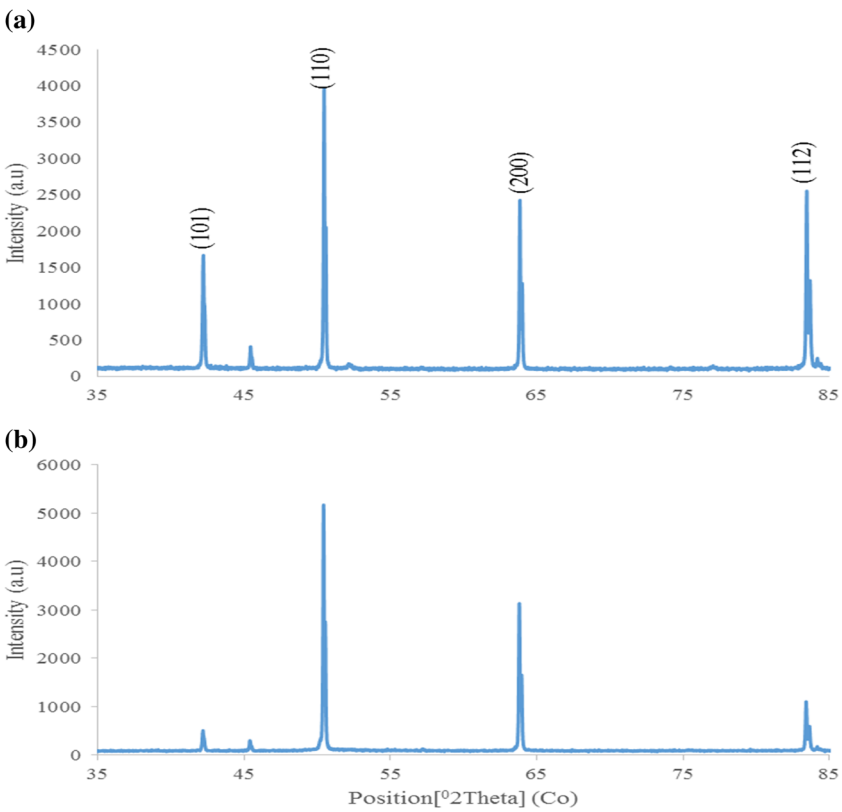

Fig. 6 XRD diffractograms of **a** Zn coating and **b** ZAC1 nanocomposite coating

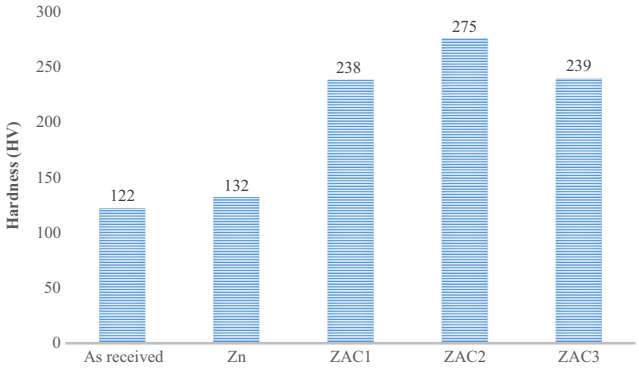

Fig. 7 Microhardness values as received sample, plain Zn coating, and ZAC nanocomposite coatings

3.3 Effect of particle loading on microhardness

Bath particle loading is one of the major factors that affect particle incorporation into a metal matrix which in turn has an effect on its microhardness property. Figure 7 shows the microhardness values of Zn coating and ZAC1, ZAC2, and ZAC3 nanocomposite coatings. The composite alloys show better microhardness values than pure Zn coating. The presence of embedded Cr_2O_3 and Al_2O_3 particles has been reported to improve the microhardness property of a metal matrix [7, 8]. Incorporated particles hinder easy movement of dislocations in a matrix and hence improved microhardness yield for composites as compared to the Zn matrix. Therefore, the higher microhardness values obtained from the composite electrodeposits can be attributed to the incorporation of nano-Cr_2O_3 and Al_2O_3 particles into the Zn metal matrix. Increasing particle content of both oxides in the bath from 2.5 to 5 g/L positively affected the hardness property of the coatings, and the ZAC2 composite exhibited the highest microhardness of 275 HV. The incorporation of particles into the metal matrix is dependent on the particle content in the bath, and this is clearly explained by Guglielmi's two-step adsorption model. A higher concentration of nanoparticulates in the bath provides more number of particles for adsorption at the cathode and thus enhancement in co-deposition [12].

Table 3 Extrapolated corrosion values obtained from Tafel plots

Sample	i_{corr} (A/cm^2)	R_p (Ω)	e_{corr} (V)	Corrosion rate (mm/year)
As received	2.76E−03	55.565	−1.406	2.412
Zn	1.28E−05	957.57	−1.1282	0.017
ZAC 1	2.24E−05	912.39	−1.13037	0.0196
ZAC 2	5.28E−05	331.02	−1.20087	0.0429
ZAC 3	1.15E−03	59.773	−1.3745	1.0033

However, the results obtained in this work showed that increasing the content of particles of one oxide and reducing the other in the bath beyond optimum concentration inhibit best particle incorporation in the matrix. Incorporation beyond optimum levels leads to formation of deposits with defects and hence reduced microhardness [9].

3.4 Electrochemical studies

The corrosion behavior of the samples was investigated using linear polarization techniques. Figure 8 below shows the polarization curves for the as-received Zn and Zn composite samples obtained in a 3.65 % wt. NaCl environment. Polarization resistance (R_p), corrosion current (i_{corr}), and corrosion rate (CR) obtained by extrapolations of the Tafel slopes are listed in Table 2. Coating as received with Zn resulted in a positive shift of 0.2778 V. This indicates that Zn improves the corrosion resistance of mild steel. However, no positive shift in electrochemical potential has been obtained when nanosized Al_2O_3 and Cr_2O_3 were incorporated into the Zn matrix. The potential of the Zn matrix decreased by 0.0022 V when 2.5 g/L of Al_2O_3 and 7.5 g/L of Cr_2O_3 were added into the bath rich. A decrease in polarization resistance and an increase in corrosion current were also observed which supports the negative potential shift shown in Fig. 8. The obtained results reveal that the incorporation of the mixed-oxide composite into the Zn matrix has no positive effect on its corrosion resistance.

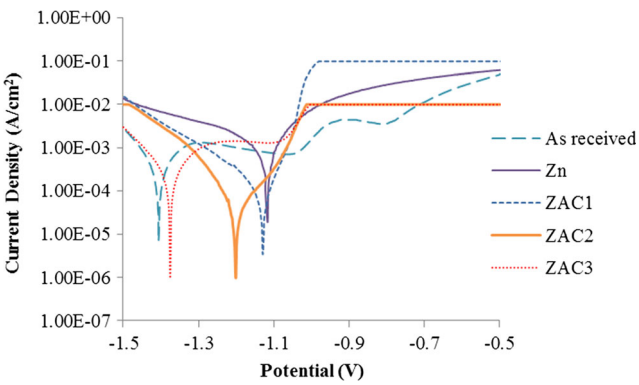

Fig. 8 Polarization curves of as-received Zn and ZAC nanocomposite coatings

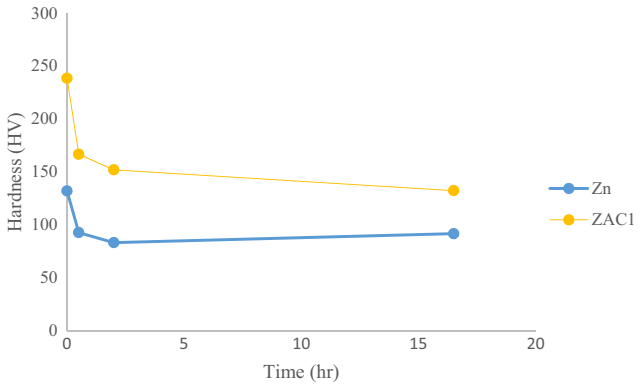

Fig. 9 Microhardness evaluation of heat-treated Zn coating and ZAC1 nanocomposite coating

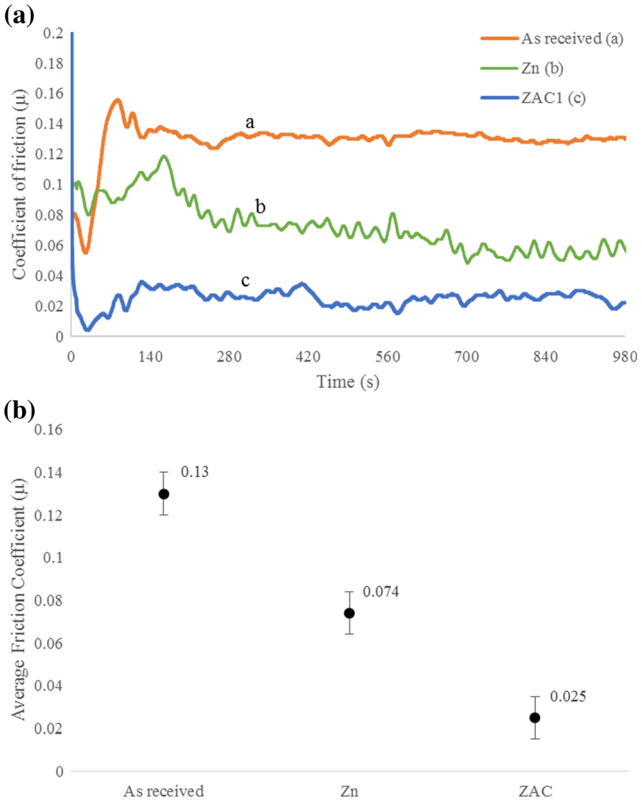

Fig. 10 Friction coefficient of the as-received sample; Zn coating and ZAC1 nanocomposite deposit **a** as function of time, and **b** average friction coefficient values

The obtained EDS results showed that the content of Cr_2O_3 (2.2 % wt.) in the coatings was higher than that of Al_2O_3 (1.0 % wt.) in ZAC1. This result suggests that Cr_2O_3 particles are easily incorporated into the metal matrix than are Al_2O_3 particles. The presence of Cr_2O_3 particles in the plating bath may inhibit the optimum incorporation of Al_2O_3 into the Zn matrix. The incorporation of Cr_2O_3 has been reported not to have a significant effect on the corrosion resistance of a metal matrix. On the other hand, adsorbed particles of Al_2O_3 improve the electrochemical properties of Zn coatings. Therefore, Al_2O_3 particles are more corrosion-resistant than are Cr_2O_3 particles [8, 9]. It can be concluded that co-deposition of Al_2O_3 and Cr_2O_3 with Zn has no positive synergetic effect on the corrosion resistance of Zn matrix (Table 3).

3.5 Thermal stability

The thermal stability of the Zn and Zn-2.5 g Al_2O_3–7.5 g Cr_2O_3 (ZAC1) electrodeposits has been evaluated by following the microhardness evolution of the deposits as revealed in Fig. 6. The deposits were exposed to heat treatment conditions at annealing temperature of 250 °C in an air circulation tube furnace for durations of 0.5, 2, and 16 h (Fig. 9).

The figure shows that heat treatment has a major influence on the thermal stability of the coatings. Drastic reduction in microhardness values of Zn coating and the composite alloy was observed in the first 30 min of exposure to heat treatment. The softening effect induced by heat treatment promotes rapid grain growth and hence reduced microhardness results. Another factor that contributes to the mechanical weakening of the coatings can be surface oxidation which is triggered by exposure to air-circulated and high-temperature environments [19]. The percentage microhardness reduction of the particle free coating and the composite alloy for the first 2 h of heat treatment is almost the same (36 and 37 %, respectively). However, the

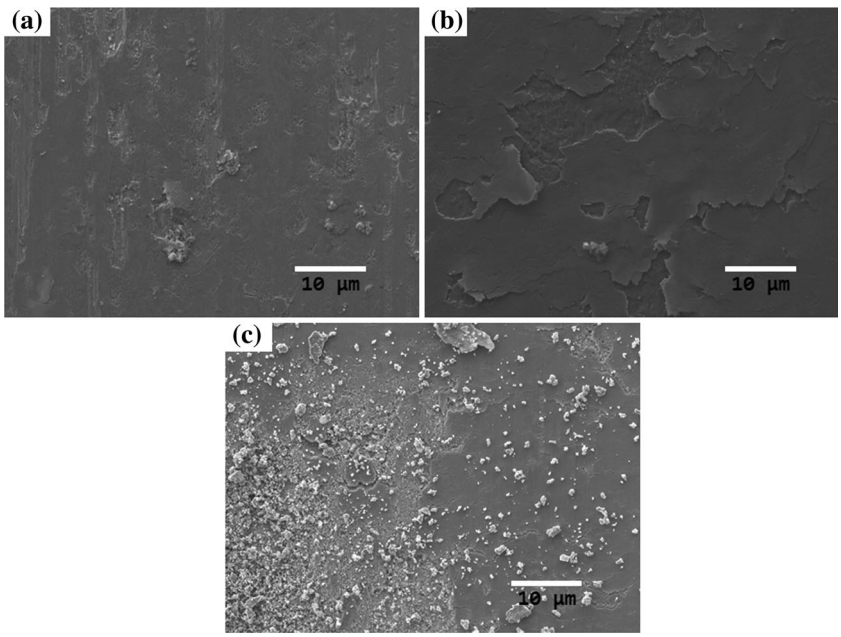

Fig. 11 Micrographs of wornout surfaces. **a** As-received sample, **b** plain Zn coating, and **c** ZAC1 nanocomposite coating

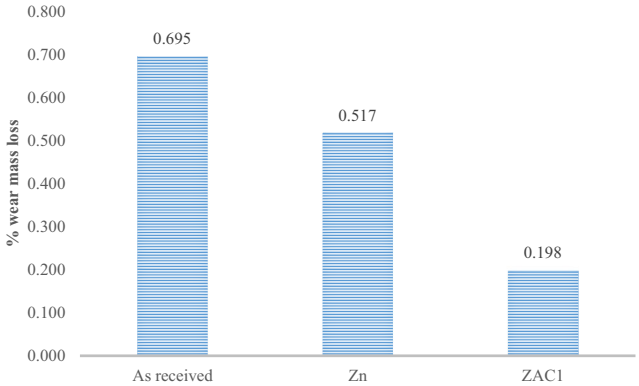

Fig. 12 Percentage of wear loss of the as-received sample, Zn coating, and ZAC1 nanocomposite coating

composite retains higher microhardness values than does pure Zn. This result is attributed to the presence of Cr_2O_3 and Al_2O_3 nanoparticles in the Zn matrix and their ability to pin the grain boundaries in the composite coating. Further exposure to heating up to 16.5 h resulted in stability in microhardness of the deposits. The composite coating retained higher microhardness values than does pure Zn deposit throughout the tests.

3.6 Tribological behavior

The evaluation of tribological properties of surface coatings is necessary for their industrial applications. Figure 10 reveals the tribological behavior of as-received Zn and ZAC samples that were evaluated at a constant normal load of 5 N for a maximum duration of 1000 s under dry reciprocating sliding conditions.

According to this figure, the coefficient of friction of Zn and ZAC electrodeposits was lower than that of the as-received sample. ZAC1 exhibits the lowest friction coefficient throughout the investigation and thus infers that these coatings possess the best lubricating properties in comparison with the other samples. The presence of ceramic nanoparticulates in the Zn matrix reduces the number of dislocation movements and results in improvement of plastic deformation resistance, thus minimizing wear volume loss. Inclusion of reinforcement materials in a metal matrix also forms a boundary between the wearing medium and matrix, thus offering good protection against wears [10]. Therefore, reduction in friction coefficient in this investigation can be ascribed to the incorporation of Cr_2O_3 and Al_2O_3 nanoparticulates in the Zn matrix. Reduction in friction coefficient can also be attributed to the possible formation of the ZnO lubricating film and the generation of wear debris.

As it can be seen in Fig. 11, the wear damage of ZAC1 is minimal compared to the amount of grooves and material loss exhibited by Zn and as-received samples. The tribological behavior of electrodeposited coatings depends on the quantity of the incorporated particles and the microstructure of the metal matrix [2]. Therefore, the wear performance of ZAC1 nanocomposite coating can be attributed to the fine microstructure with uniform and compact grains as depicted in Fig. 2b.

The percentage weight loss of the deposits obtained under non-lubricating sliding at a normal load of 5 N and speed of 200 rev/min is shown in Fig. 12. The composite coating exhibited the lowest percentage weight loss of 0.198 % as compared to 0.695 and 0.517 % of the as-received sample and plain Zn coating, respectively. The drastic reduction in wear loss shown by the composite deposit can be ascribed to the inclusion of Al_2O_3 and Cr_2O_3 nanoparticles into the Zn matrix. The presence of nanoparticles provides a lubricating barrier between the matrix and the wearing medium, thus reducing the magnitude of wear of the composite [10, 13]. Therefore, the improvement in wear resistance of the composite coating owes to the excellent self-lubrication exhibited by these particles. This result supports the friction behavior displayed by the composite sample.

Table 4 Experimental results

Run order	Hardness (HV)	Corrosion rate (mm/year)	Wear loss (%)
(AS)	122	2.4120	0.6950
(Zn)	132	0.0170	0.5170
(ZAC1)	238	0.0196	0.1980
(ZAC2)	275	0.0429	0.0000
(ZAC3)	239	1.0033	0.0000

Table 5 Grey normalized values

Grey model normalized values			
Run order	Hardness (HV)	CR (mm/year)	Wear loss (%)
AS	0.0000	0.0000	0.0000
Zn	0.0654	1.0000	0.2561
ZAC1	0.7582	0.9989	0.7151
ZAC2	1.0000	0.9892	1.0000
ZAC3	0.7647	0.5882	1.0000

Table 6 Grey relational analysis

Grey relational analysis (Δ_{oi})			
Run order	Hardness (HV)	CR (mm/yearr)	Wear loss (%)
AS	1.0000	1.0000	1.0000
Zn	0.9346	0.0000	0.7439
ZAC1	0.2418	0.0011	0.2849
ZAC2	0.0000	0.0108	0.0000
ZAC3	0.2353	0.4118	0.0000

Table 7 Grey relational coefficient and Grey relational grade

Grey relational coefficient ($\xi_i(k)$)				Grey relational grade (γ)
Run order	Hardness (HV)	CR (mm/year)	Wear loss (%)	
AS	0.3333	0.3333	0.3333	0.3333
Zn	0.3485	1.0000	0.4020	0.5835
ZAC1	0.6740	0.9978	0.6370	0.7696
ZAC2	1.0000	0.9789	1.0000	0.9930
ZAC3	0.6800	0.5484	1.0000	0.7428

4 Numerical analysis for gray relational model

4.1 Grey relational analysis

In the Grey relational analysis, experimental data, i.e., measured responses, are first normalized in the range of 0 to 1. This process is called Grey relational generation. Based on this data, Grey relational coefficients are calculated to represent the correlation between the ideal (best) and the actual normalized experimental data. Overall, the Grey relational grade is determined by averaging the grey relational coefficient corresponding to selected responses. The overall quality characteristics of the multi-response process depend on the calculated grey relational grade.

4.2 Grey relational generation

In Grey relational generation, the normalized values corresponding to the smaller-the-better (SB) criterion which can be expressed as

$$x_i(k) = \frac{\max y_i(k) - y_i(k)}{\max y_i(k) - \min y_i(k)} \tag{1}$$

The larger-the-better criterion can also be expressed as

$$x_i(k) = \frac{y_i(k) - \min y_i(k)}{\max y_i(k) - \min y_i(k)} \tag{2}$$

where $x_i(k)$ is the normalized value after the Grey relational generation, $\min y_i(k)$ is the smallest value of $y_i(k)$ for the k^{th} response, and $\max y_i(k)$ is the largest value of $y_i(k)$ for the k^{th} response [14]. An ideal sequence is $[x_0(k)(k=1,2,3.....5)]$ for the responses.

4.3 Grey relational coefficient and Grey relational grade

The Grey relational coefficient $\xi_i(k)$ can be calculated as

$$\xi_i(k) = \frac{\Delta_{\min} - \psi\Delta_{\max}}{\Delta_{oi}(k) + \psi\Delta_{\max}} \tag{3}$$

where $\Delta_{oi} = \|x_o(k) - x_i(k)\|$ is the absolute value of the difference of $x_o(k)$ and $x_i(k)$; ψ is the distinguishing coefficient $0 \le \psi \le 1$. $\psi = 0.5$ is generally used.

$\Delta_{\min} = \forall j^{\min} \in i \, \forall k^{\min} \|x_o(k) - x_j(k)\|$ is the smallest value of Δ_{oi}, and $\Delta_{\max} = \forall j^{\max} \in i \, \forall k^{\max} \|x_o(k) - x_j(k)\|$ is the largest value of Δ_{oi}.

After averaging the Grey relational coefficients, the Grey relational grade γ_i can be computed as

$$\gamma_i = \frac{1}{n}\sum_{k=1}^{n} \xi_i(k) \tag{4}$$

where n is the number of process responses. The higher value of the Grey relational grade corresponds to the intense relational degree between the reference sequence $x_o(k)$ and the given sequence $x_o(k)$.

The reference sequence $x_o(k)$ represents the best process sequence. Therefore, a higher Grey relational grade means that the corresponding parameter combination is closer to the optimal [14]. The mean response for the Grey relational grade with its grand mean and the main effect plot of Grey relational grade are very important because optimal process conditions can be evaluated from this plot [14] (Tables 4, 5, and 6).

According to the experimental design, it is clearly observed from Table 7 that run order 4 (ZAC2) with hardness of 275 HV and corrosion rate of 0.0429 mm/year has the highest Grey relational grade of 0.9930. This model corresponds with the experimental results. Since the experimental design is orthogonal, it is then possible to see the effects of Al_2O_3 and Cr_2O_3 on the hardness and corrosion rate values. The experimental results showed that increasing the content of particles of one oxide and reducing the other in the bath at optimum concentration yielded the highest hardness value which corresponds with the numerical model and inhibits best particle

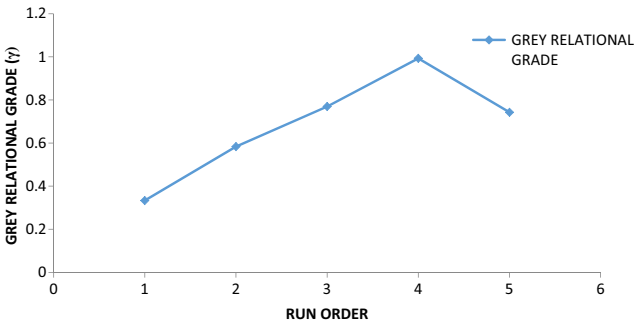

Fig. 13 Grey relational grade

incorporation in the matrix. Incorporation beyond optimum levels leads to formation of deposits with defects [15] and hence reduces the hardness and increases the corrosion rate by 21.5 %. The mean of the relational grade for each level of the hardness, corrosion rate, and wear is summarized in the multi-response performance index table (Table 7). Coated samples ZAC1, ZAC2, and ZAC3 have higher Grey relational grade values than uncoated samples which indicate the influence of Al_2O_3 and Cr_2O_3 powder coatings on the substrate. In addition, the total mean of the Grey relational grade of the three experiments is also calculated, as shown in Table 7. In contrast, Fig. 13 shows the Grey relational grade. Basically, the larger the Grey relational grade is, the closer will be the product quality to the ideal value. Thus, the larger the Grey relational grade is desired. Since the Grey relational grades represented the level of correlation between the reference and comparability sequences, the larger Grey relational grade means that the comparability sequence exhibits a stronger correlation with reference sequence.

5 Conclusions

Zn-Al_2O_3-Cr_2O_3 nanocomposite coatings were successfully prepared by electrodeposition technique onto mild steel substrates. The surface morphology of the composite coatings showed granular-like crystals compared to the Zn flake-like crystalline structure, thus proving that Al_2O_3 and Cr_2O_3 incorporation into the Zn matrix has a significant effect on its microstructure. The microstructure exhibited by the composite revealed surface defects that can be attributed to its poor corrosion performance. The incorporation of the mixed oxide composite had no significant effect on the corrosion resistance of Zn coatings. However, the microhardness value and thermal stability of the composite coatings showed positive results up to 16 h at 250 °C of heat treatment. Reduction in coefficient of friction proved the coatings to possess self-lubricating properties and hence improvement in wear resistance. This investigation revealed that the incorporation of the mixed oxide composite into the Zn matrix has a positive synergetic effect on the microhardness, thermal stability, and tribology but not on the corrosion resistance. Finally, the Grey relational model results were checked with experimental results and a good agreement was found.

Acknowledgment This material is based upon work supported financially by the National Research Foundation. The equipment supported by the Surface Engineering Research Centre (SERC) Tshwane University of Technology, Pretoria, is deeply appreciated.

References

1. Khan WS, Asmatulu R (2013) Nanotechnology emerging trends, markets, and concerns. Nanotechnology safety. Elsevier, Amsterdam, pp. 1–16
2. Chen L, Wang L, Zeng Z, Xu T (2006) Surf Coat Technol 201: 599–605
3. Ranganatha S, Venkatesha TV, Vathsala K, Punith kumar MK (2012) Surf Coat Technol 208:64–72
4. Vathsala K, Venkatesha TV (2011) Appl Surf Sci 257:8929–8936
5. Praveen BM, Venkatesha TV (2011) Inter J Electrochem 2011:1–4
6. Zheng H, An M (2008) J Alloys Compd 459:548–552
7. Sancakoglu O, Culha O, Toparli M, Agaday B, Celik E (2011) Mater Design 32:4054–4061
8. Srivastava M, Balaraju JN, Ravishankar B, Rajam K (2010) Surf Coat Technol 205:66–75
9. Blejan D, Muresan LM (2012) Mater Corr 63:1–5
10. Saha RK, Khan TI (2010) Surf Coat Technol 205:890–895
11. Hamid ZA, El-Sheikh M (2013) J Met Eng 2:71–79
12. Lee CK (2012) Tribology Inter. 55:7–14
13. Sylla D, Creus J, Savall C, Roggy O, Gadouleau M, Refait P (2003) Thin Solid Films 424:171–178
14. Datta S, Bandyopadhyay A, Pal PK (2008) Int J Adv Manu Tech 39:1136–1143
15. Adebiyi DI, Popoola API, Botef I (2016) Metals 6:135. doi:10.3390/met6060135
16. Popoola API, Fayomi OSI (2011) Inter J Electrochem Sci 6: 3254–3263
17. Aruna ST, William Grips VK, Rajam KS (2009) J Alloys Compds 468:546–552
18. Fayomi OSI, Popoola API, Aigbodion VS (2014) J of Alloy and Compd 617:455–463
19. Fayomi OSI, Popoola API, Oloruntoba DT (2016) Protection of Metals and Physical Chemistry of Surfaces 52(3):512–516